Simulation of the density of states in isothermal and adiabatic ensembles

Fernando A. Escobedo
School of Chemical and Biomolecular Engineering, Cornell University, Ithaca, New York 14853, USA
(Received 4 February 2006; published 8 May 2006)

This paper provides a unified treatment of the fundamental methods used to obtain the density of states ω via molecular simulations with isothermal ensembles (IEs) and adiabatic ensembles (AEs). Our analysis and results show that ω provides a natural bridge to go back and forth between IE and AE simulation data. They also underline the difference between the density of states of potential energy macrostates ω and that of total energy macrostates Ω, even though both provide access to the thermodynamic properties of the system. Visited-states approaches and transition matrix methods are described and applied to the Lennard-Jones fluid to target ω and Ω as functions of energy and volume macrostates. It is shown that one can obtain ω via a generalized acceptance-ratio formula that is applicable regardless of the conditions at which the ensemble is simulated. In this way, one can obtain ω while performing conventional IE or AE simulations, and do it at no extra cost and with a higher accuracy than is achievable with histogram methods.

DOI: 10.1103/PhysRevE.73.056701 PACS number(s): 02.70.Tt, 05.10.Ln, 02.70.−c

I. INTRODUCTION

Molecular simulations with conventional statistical mechanical ensembles are still the main route to access the thermodynamic properties of a system [1,2]. In such simulations, one primarily collects information about ensemble averages of key quantities of the system which can, directly or indirectly, be connected to macroscopic, thermodynamic properties. Such key quantities will be denoted macrostate variables or macrovariables and are extensive properties that fluctuate in the simulation. In recent years, it has been recognized that simulation methods able to extract density of states ω data (as a function of the macrovariables) are particularly efficient in mapping out thermodynamic properties over broad ranges of conditions [1–10]. Ensemble averages can be easily obtained from ω by using straightforward statistical mechanical formulas. One of the best-known approaches relies on estimating ω from the histogram(s) that record(s) the variations of the ensemble macrovariables [3]. In practice, multiple histograms, corresponding to simulations at different state points, are collected and combined via the multihistogram reweighting (MHR) method [4]; ω is extracted (within a multiplicative factor) that is usable over the macrovariable domain sampled during the simulations. Often, ω itself is not obtained or reported but remains implicit in the equations used for reweighing the thermodynamic properties of interest. In some applications, a free-energy function $\mathfrak{I}$, rather than ω, is the property of interest or is the underlying function that allows the reweighting [9–16]. MHR is a "visited-states" method in that ω or $\mathfrak{I}$ comes from data on the frequency with which the system visited different macrostates. More recently, another class of methods has been developed wherein one gets ω or $\mathfrak{I}$ not from histogram data but from data on the attempted transitions between macrostates [17–25]. Such transition probability or transition matrix (TM) methods have been shown to be more robust and accurate than visited-states methods but, as of now, are still far less popular than visited-states methods.

The methods described above have been extensively used with isothermal ensembles (IEs), i.e., those where the temperature is fixed in the simulation. The MHR method has been used with the canonical and grand canonical ensembles [2–8,16]. TM methods have been used, for example, with the canonical ensemble as the core from which $\mathfrak{I}$ functions are generated and reweighted to get properties associated with grand canonical, isobaric-isothermal, and semigrand ensembles [20–25]. Recently [26], it has been shown that MHR and a particular type of TM method can also be used with any adiabatic ensemble (AE), i.e., ensembles where the system is not in contact with a thermal bath and therefore the temperature is not fixed [26–28]. Aside from the microcanonical ensemble or *NVE* ensemble, AEs are not as well known or easy to implement as IEs but have been used in a number of studies (see, for example, Refs. [26–42]). The practical relevance of AEs may increase in the future as thermally insulated, small systems can be experimentally realized in microenvironments.

Because ω does not depend on thermodynamic fields, there also exist iterative schemes, like the multicanonical [43,44], entropy [45], density of states [46–49], and TM uniform ensemble [20,50,51] methods, that can target ω in a system without the need of specifying an ensemble, just the constraints on the values of some extensive properties (e.g., to fix the size of the system). In such a case, the distinction between an IE and an AE vanishes. Such ensemble-weight-independent methods, which can make use of either visited-states or TM methods to estimate ω, have been extensively described elsewhere and will not be reviewed here. Instead, we focus on methods to target ω that do depend on the specification and simulation of an ensemble (that can be isothermal or adiabatic). Both ensemble-weight-independent and ensemble-weight-dependent routes to ω are important because both are extensively used, have complementary strengths, and the best choice is often system dependent. Ensemble-weight-independent methods, e.g., work better for unidimensional paths (when ω is mapped out as a function of a single varying property), require some preliminary work with conventional ensembles to identify the relevant macrovariable domain, and involve an iterative scheme to converge. Ensemble-weight-dependent methods, on the other hand, work well even with multidimensional paths, are often easily set up since the relevant macrovariable domain

"follows" from the specification of thermodynamic states, and can be less iterative.

The goal of this paper is thus to provide a unified framework for the (ensemble-weight-dependent) simulation of ω and $\mathfrak{I}$ with IEs and AEs. Both MHR and TM methods are described that can be equally used with IEs and AEs to generate ω. In particular, it is shown how by simulating multiple state points with any conventional IE or AE, one can advantageously use a TM scheme to generate ω with higher accuracy than using MHR. Several proof-of-principle examples are presented using the Lennard-Jones system as testbed, primarily to illustrate how simulations with the less-known AEs can be used to generate different types of density of states functions and to pinpoint phase coexistence. These applications also underline some possible advantages of AEs over IEs.

II. FORMULATION OF ISOTHERMAL AND ADIABATIC ENSEMBLES

In Refs. [26,52] we described suitable notations to represent generalized IEs and AEs, respectively. Those notations were not the same since their main purpose was conciseness. For this discussion, however, we adopt the notation used in Ref. [26] for both AEs and IEs. Let us denote as E the total energy and as U the potential energy of the system, so that $E=U+K$ where K is the kinetic energy. Let us also define the set of extensive properties $\mathbf{Y}=\{V,N_1,\ldots,N_c\}$ and the set of conjugate extensive fields $\mathbf{f}=\{-P,\mu_1,\ldots,\mu_c\}$, where V is the volume, N_i is the number of molecules of species i, P is the pressure, and μ_i is the chemical potential of component i. The fundamental thermodynamic equation

$$dE = T\,dS - P\,dV + \sum_{i=1}^{c} \mu_i dN_i$$

becomes

$$dE = T\,dS + \mathbf{f}\cdot\mathbf{dY}. \tag{1}$$

Clearly

$$f_i = (\partial E/\partial Y_i)_{S,Y_{j\neq i}}$$

and since

$$E = TS + \mathbf{f}\cdot\mathbf{Y}, \tag{2}$$

the Gibbs-Duhem equation takes the form $0=S\,dT+\mathbf{Y}\cdot\mathbf{df}$. The total density of macrostates can be written by factoring out its ideal-gas and "excess" contributions:

$$\begin{aligned}\omega_{tot}(K,U,\mathbf{Y}) &= \omega_{ig}(K,\mathbf{Y})\omega_{ex}(U,\mathbf{Y}) \\ &= \varpi_{ig}^{AE}(\mathbf{Y})K^{F/2-1}\Theta(K)\omega_{ex}(U,\mathbf{Y})\end{aligned} \tag{3}$$

where F is the number of degrees of freedom, and

$$\varpi_{ig}^{AE} = \frac{V^N}{\Gamma(F/2)}\prod_{i=1}^{c}\frac{a_i^{N_i}}{N_i!} \tag{4}$$

where Γ is the gamma function and a_i is a constant specific to component i [e.g., for a single-site particle $a_i=(2\pi m_i/\hbar^2)^{3/2}$ where m_i is the mass and $\hbar$ is de Broglie's wavelength]. The step function Θ in Eq. (3) simply constrains K to have positive values.

In specifying different ensembles, we are basically setting alternative representations of thermodynamic states which can be suitably described by using Legendre transformations. This has been explained in detail in [26,52]. Here we simply summarize the key results. In any given ensemble, we can identify some key extensive properties that, by construction, are fixed and some that are allowed to fluctuate: the fixed ones are called $\bar{\mathbf{Y}}$ (a subset of $\mathbf{Y}$), while the fluctuating ones are $\{U,\tilde{\mathbf{Y}}\}$ where $\tilde{\mathbf{Y}}$ is the "rest" of the Y variables, i.e., $\tilde{\mathbf{Y}}\cup\bar{\mathbf{Y}}=\mathbf{Y}$. The fluctuations in $\tilde{\mathbf{Y}}$ are "controlled" by specifying (fixing) the corresponding conjugate f fields which are placed in $\bar{\mathbf{f}}$ (a subset of $\mathbf{f}$ so that $\tilde{\mathbf{f}}\cup\bar{\mathbf{f}}=\mathbf{f}$). The fluctuations in U are controlled by specifying (fixing) a further "special" property which we will denote as D. For IEs, $D=\beta=1/\mathrm{kT}$ (k is Boltzmann's constant), while for AEs it is an extensive property defined by

$$D = D_{AE} = E - \tilde{\mathbf{f}}\cdot\tilde{\mathbf{Y}} \quad \text{(AE only)}. \tag{5}$$

Consistent with Eq. (3), the probability of $\{K,U,\tilde{\mathbf{Y}}\}$ *macrostates* for an AE specified by the properties being fixed ($\bar{\mathbf{Y}}$, $\tilde{\mathbf{f}}$, and D) is

$$\Pi(K,U,\tilde{\mathbf{Y}}|D,\bar{\mathbf{Y}},\tilde{\mathbf{f}}) = \Pi(U,\tilde{\mathbf{Y}}|D,\bar{\mathbf{Y}},\tilde{\mathbf{f}}) \propto \omega_{tot}(U,\tilde{\mathbf{Y}}|\bar{\mathbf{Y}}), \tag{6}$$

where the K dependence of Π became implicit in $\{U,\mathbf{Y}\}$ given that

$$K = D - U + \tilde{\mathbf{f}}\cdot\tilde{\mathbf{Y}} \quad \text{(AE only)}. \tag{7}$$

For an IE, the probability of $\{K,U,\tilde{\mathbf{Y}}\}$ macrostates results from multiplying ω_{tot} by the appropriate ensemble Boltzmann factor:

$$\Pi(K,U,\tilde{\mathbf{Y}}|\beta,\bar{\mathbf{Y}},\tilde{\mathbf{f}}) \propto \omega_{tot}(K,U,\tilde{\mathbf{Y}}|\bar{\mathbf{Y}})\exp[-\beta(E-\tilde{\mathbf{f}}\cdot\tilde{\mathbf{Y}})]. \tag{8}$$

Substituting Eq. (3) into Eq. (8), integrating over K, and recalling that $\int_0^\infty K^{F/2-1}\exp(-\beta K)dK=\beta^{-F/2}\Gamma(F/2)$, we get

$$\Pi(U,\tilde{\mathbf{Y}}|\beta,\bar{\mathbf{Y}},\tilde{\mathbf{f}}) \propto \varpi_{ig}^{IE}(\tilde{\mathbf{Y}}|\bar{\mathbf{Y}})\omega_{ex}(U,\tilde{\mathbf{Y}}|\bar{\mathbf{Y}})\exp[-\beta(U-\tilde{\mathbf{f}}\cdot\tilde{\mathbf{Y}})] \tag{9}$$

where

$$\varpi_{ig}^{IE} = V^N\prod_{i=1}^{c}\frac{(a_i\beta^{-3/2})^{N_i}}{N_i!}. \tag{10}$$

Equations (3), (6), and (9) allow us to write a general expression for the probability of $\{U,\tilde{\mathbf{Y}}\}$ macrostates for any such IE or AE as

$$\Pi(U,\tilde{\mathbf{Y}}|D,\tilde{\mathbf{f}},\bar{\mathbf{Y}}) \propto \omega(U,\tilde{\mathbf{Y}}|\bar{\mathbf{Y}})W(U,\tilde{\mathbf{Y}}|D,\tilde{\mathbf{f}}) \tag{11}$$

where ω is a configurational density of states,

TABLE I. Summary of ensemble formulas. a, substance-specific constant, F, number of degrees of freedom, Γ, gamma function, Θ, unit step function, K, kinetic energy, E, total energy, U, potential energy, V, volume, N, number of molecules, μ chemical potential, P, pressure, W, ensemble weight, and Q, partition function. $\Phi = U - \tilde{\mathbf{f}}\cdot\tilde{\mathbf{Y}}$, $\tilde{\mathbf{f}}\cup\bar{\mathbf{f}} = \mathbf{f} = \{-P, \mu_1, \ldots, \mu_c\}$, and $\tilde{\mathbf{Y}}\cup\bar{\mathbf{Y}} = \mathbf{Y} = \{V, N_1, \ldots, N_c\}$. In any ensemble, properties $\tilde{\mathbf{f}}$ (a subset of $\mathbf{f}$), $\bar{\mathbf{Y}}$ (a subset of $\mathbf{Y}$), and D are fixed.

Isothermal ensembles	Adiabatic ensembles
$D = \beta = 1/kT$	$D = E + \Phi - U$
$W = \exp(-\beta\Phi)$	$W = K^{F/2-1}\Theta(K) \quad K = D - \Phi$
$\varpi_{ig} = V^N \prod_{i=1}^{c} \frac{(a_i \beta^{-3/2})^{N_i}}{N_i!}$	$\varpi_{ig} = \frac{V^N}{\Gamma(F/2)} \prod_{i=1}^{c} \frac{a_i^{N_i}}{N_i!}$
$\ln Q = \mathfrak{I} = -D\bar{\mathbf{f}}\cdot\bar{\mathbf{Y}}$	$\ln Q = \ln \Omega = \mathfrak{I} = S/k$
Examples (always $D = \beta$)	Examples (always $\mathfrak{I} = S/k$)
NVT ensemble	*NVE* ensemble
$\bar{\mathbf{Y}} = \{N, V\} \quad \tilde{\mathbf{Y}} = 0 \quad \tilde{\mathbf{f}} = 0 \quad \mathfrak{I} = -\beta A$	$D = E \quad \bar{\mathbf{Y}} = \{N, V\} \quad \tilde{\mathbf{Y}} = 0 \quad \tilde{\mathbf{f}} = 0$
$W = \exp(-\beta U)$	$W = (E - U)^{F/2-1}\Theta(E - U)$
NPT ensemble	*NPH* ensemble
$\bar{\mathbf{Y}} = N, \tilde{\mathbf{Y}} = V, \tilde{\mathbf{f}} = -P, \mathfrak{I} = -\beta G$	$D = H \quad \bar{\mathbf{Y}} = N \quad \tilde{\mathbf{Y}} = V \quad \tilde{\mathbf{f}} = -P$
$W = \exp[-\beta(U + PV)]$	$W = (H - U - PV)^{F/2-1}\Theta(H - U - PV)$
μVT ensemble	μVL ensemble
$\bar{\mathbf{Y}} = V, \tilde{\mathbf{Y}} = N, \tilde{\mathbf{f}} = \mu, \mathfrak{I} = \beta PV$	$D = L = E - \mu N \quad \bar{\mathbf{Y}} = V \quad \tilde{\mathbf{Y}} = N \quad \tilde{\mathbf{f}} = \mu$
$W = \exp[-\beta(U - \mu N)]$	$W = (L - U + \mu N)^{F/2-1}\Theta(L - U + \mu N)$

$$\omega(U, \tilde{\mathbf{Y}}|\bar{\mathbf{Y}}) = \varpi_{ig}(\tilde{\mathbf{Y}}|\bar{\mathbf{Y}})\omega_{ex}(U, \tilde{\mathbf{Y}}|\bar{\mathbf{Y}}) \tag{12}$$

where for ϖ_{ig} one uses Eq. (4) or (10) depending on the ensemble type (AE or IE, respectively). In Eq. (11), W is an ensemble weight function given by

$$W = \begin{cases} \exp(-\beta\Phi) & \text{for IEs,} \\ (D - \Phi)^{F/2-1}\Theta(D - \Phi) & \text{for AEs,} \end{cases} \tag{13}$$

where $\Phi = U - \tilde{\mathbf{f}}\cdot\tilde{\mathbf{Y}}$. Likewise, the probability of a particular microstate or configuration $\gamma = \{\mathbf{r}, \tilde{\mathbf{Y}}\}$ where $\mathbf{r}$ is the set of atomic coordinates is

$$p(\gamma|D, \bar{\mathbf{Y}}, \tilde{\mathbf{f}}) \propto \varpi_{ig}(\tilde{\mathbf{Y}}|\bar{\mathbf{Y}})W[U(\mathbf{r}), \tilde{\mathbf{Y}}|D, \tilde{\mathbf{f}}] \tag{14}$$

where again ϖ_{ig} is given by Eq. (4) (for AEs) or Eq. (10) (for IEs). Table I summarizes the expressions for ϖ_{ig} and W in AEs and IEs. It should be noted, however, that in simulations, W often absorbs some of the terms in ϖ_{ig} so that all properties needed are "configurational" quantities; explicit equations that account for this have been presented in Ref. [9]. The generalized partition function Q is given by integration of either Eq. (11),

$$Q(D, \bar{\mathbf{Y}}, \tilde{\mathbf{f}}) = \int_{U, \tilde{\mathbf{Y}}} dU\, d\tilde{\mathbf{Y}}\ \omega(U, \tilde{\mathbf{Y}}|\bar{\mathbf{Y}})W(U, \tilde{\mathbf{Y}}|D, \tilde{\mathbf{f}}), \tag{15}$$

or Eq. (14),

$$Q(D, \bar{\mathbf{Y}}, \tilde{\mathbf{f}}) = \int_{\tilde{\mathbf{Y}}} d\tilde{\mathbf{Y}}\ \varpi_{ig}(\tilde{\mathbf{Y}}|\bar{\mathbf{Y}}) \int_{\mathbf{z}} d\mathbf{z}\ W[U(\mathbf{z}), \tilde{\mathbf{Y}}|D, \tilde{\mathbf{f}}], \tag{15'}$$

where $\mathbf{z}$ is the set of reduced particle coordinates. The thermodynamic bridge function $\mathfrak{I}$ is

$$\mathfrak{I} = \ln Q(D, \bar{\mathbf{Y}}, \tilde{\mathbf{f}}). \tag{16}$$

For IEs, $\mathfrak{I}$ is related to the familiar free energies (which depend on the specific ensemble) while for AEs $\mathfrak{I}$ is always the entropy (see Table I). For both IEs and AEs, the "equilibrium" state always corresponds to a maximum in the $\mathfrak{I}$ function. That the entropy is always a maximum in AEs is readily seen by using Eqs. (1) and (5) to write the Clausius inequality as

$$dD - T\,dS + \bar{\mathbf{f}}\cdot d\bar{\mathbf{Y}} + \tilde{\mathbf{Y}}\cdot d\tilde{\mathbf{f}} \leqslant 0,$$

and since by construction $\bar{\mathbf{Y}}$, $\tilde{\mathbf{f}}$, and D are fixed in the AE, it follows that $dS \geqslant 0$. At equilibrium, the adiabatic condition ($\delta q = dS/T = 0$) implies $dS = 0$.

Multiensemble (ME) approaches involve an extended partition function that combines different systems, each defined by the same type of partition function $Q(D, \bar{\mathbf{Y}}, \tilde{\mathbf{f}})$ but for different conditions (states) wherein one or several of those properties in $\{D, \bar{\mathbf{Y}}, \tilde{\mathbf{f}}\}$ change from one ensemble to the next. If the set of variables that define each system in the ME scheme is called λ,

$$\lambda_i \in \{D_i, \bar{\mathbf{Y}}_i, \tilde{\mathbf{f}}_i\} \tag{17}$$

then each single-system "partition function" in the ME can be denoted as $Q_i = Q(\lambda_i)$, with each Q fully defined by Eq. (15). ME approaches can be classified into parallel MEs (or "replica exchange" methods) [14–16] and serial MEs like expanded-ensemble methods [11–13].

III. SIMULATION OF THE DENSITY OF STATES

There exist many iterative schemes (like the multicanonical and uniform-ensemble sampling [43–51]) that can target $\omega(U, \tilde{\mathbf{Y}} | \bar{\mathbf{Y}})$ in a system without fully specifying an ensemble, just the constraints in $\bar{\mathbf{Y}}$. But as indicated in Sec. I, such ensemble-weight-independent methods lie beyond the scope of this work. Here we restrict ourselves to ensemble-weight-dependent routes to ω or ω_{ex}, noting that ω and ω_{ex} are trivially related via Eq. (12). In principle any method used to extract ω with an IE should also be applicable to an AE and in Secs. III B and III C, we will review two such general methods. But first, we clarify the distinction between ω and other density of states functions.

A. Relating AEs and IEs via the density of states

The partition function of an AE can be associated with a density of states function, to be denoted Ω. If we write Eq. (15) for an AE we have

$$\Omega(D, \bar{\mathbf{Y}}, \tilde{\mathbf{f}}) = \int_{U,\tilde{\mathbf{Y}}} dU\, d\tilde{\mathbf{Y}}\; \omega_{tot}(U, \tilde{\mathbf{Y}} | \bar{\mathbf{Y}}) = \int_{U,\tilde{\mathbf{Y}}} dU\, d\tilde{\mathbf{Y}}\; \omega(U, \tilde{\mathbf{Y}} | \bar{\mathbf{Y}}) W. \tag{18}$$

Clearly Ω and ω in Eq. (18) are different in that ω describes the degeneracy of macrostates defined (at least partially) by U while Ω does not. For illustration, consider the case of a microcanonical ensemble (see Table I) for which

$$\Omega(E|N,V) = \varpi_{ig}^{AE} \int_{-\infty}^{E} dU\; \omega_{ex}(U|N,V)(E-U)^{F/2-1} \tag{19}$$

where ϖ_{ig}^{AE} is a now a constant. The notation $\Omega(E|N,V)$ highlights the constancy of N and V in the $\Omega(N,V,E)$ function. Equation (19) makes plain the key difference between two seemingly identical densities of states $\Omega(E|N,V)$ and $\omega = \varpi_{ig}^{AE}\, \omega_{ex}(U|N,V)$. The function ω_{ex} is in principle accessible through simulations in IEs or AEs; e.g., for fixed N and V, canonical and microcanonical ensemble runs can access $\omega_{ex}(U|N,V)$. Equation (19) then shows how one can get $\Omega(E|N,V)$ via numerical integration of the simulated $\omega_{ex}(U|N,V)$ data. Likewise, one could get the canonical partition function from the numerical integration of $\omega_{ex}(U|N,V)$ from

$$Q(N,V,\beta) = \varpi_{ig}^{IE} \int_{-\infty}^{\infty} dU\; \omega_{ex}(U|N,V) \exp(-\beta U). \tag{20}$$

Equations (19) and (20) reflect the fact that $\omega_{ex}(U,N,V)$ is the fundamental function that allows us to access either IE or AE partition functions and any other ensemble-related property. This conclusion follows more generally from Eqs. (11) and (12) that show that ω_{ex} is the same function (within a constant factor) *regardless of ensemble type*:

$$\begin{matrix}\text{Isothermal ensemble} \\ \text{fixed } \bar{\mathbf{Y}}\tilde{\mathbf{f}}\beta\end{matrix} \leftrightarrow \omega_{ex}(U, \tilde{\mathbf{Y}} | \bar{\mathbf{Y}}) \leftrightarrow \begin{matrix}\text{Adiabatic ensemble} \\ \text{fixed } \bar{\mathbf{Y}}\tilde{\mathbf{f}} D_{AE}\end{matrix} \tag{21}$$

Note that it is also possible to get $\omega(U|N,V)$ from $\Omega(E|N,V)$ [or from $Q(N,V,\beta)$] data but this entails solving an integral equation via an "inversion" method. For example, Eq. (19) is a Volterra equation of the first kind that can be solved for ω_{ex} via a numerical procedure [53]. Such indirect routes, however, lie beyond the scope of this work.

Finally, we present two additional AI-AE connecting equations that will be important for later reference. Using $K = E - U$ in Eq. (3), it follows from Eqs. (8) and (18) that

$$\Pi(E, \tilde{\mathbf{Y}} | \beta, \bar{\mathbf{Y}}, \tilde{\mathbf{f}}) \propto \exp[-\beta(E - \tilde{\mathbf{f}} \cdot \tilde{\mathbf{Y}})] \int_U dU\; \omega_{tot}(U, \tilde{\mathbf{Y}} | \bar{\mathbf{Y}}) \propto \exp[-\beta(E - \tilde{\mathbf{f}} \cdot \tilde{\mathbf{Y}})] \Omega(E, \tilde{\mathbf{Y}} | \bar{\mathbf{Y}}). \tag{22}$$

Likewise, using $K = D_{AE} - U + \tilde{\mathbf{f}} \cdot \tilde{\mathbf{Y}}$ in Eq. (3), it follows from Eqs. (8) and (18) that

$$\Pi(D_{AE} | \beta, \bar{\mathbf{Y}}, \tilde{\mathbf{f}}) \propto \exp(-\beta D_{AE}) \int_{U,\tilde{\mathbf{Y}}} dU\, d\tilde{\mathbf{Y}}\; \omega_{tot}(U, \tilde{\mathbf{Y}} | \bar{\mathbf{Y}}) \propto \exp(-\beta D_{AE}) \Omega(D_{AE} | \bar{\mathbf{Y}}, \tilde{\mathbf{f}}). \tag{23}$$

Equations (22) and (23) are instances wherein one can get the probability density for an IE (left-hand sides) based on information obtained in an AE simulation (Ω data).

B. Estimating ω and $\mathfrak{I}$ from visited-states or multihistogram reweighting methods

Histogram methods estimate ω from simulation data on the frequency with which the system visits different macrostates [2,4]. Reference [26] provided a general formulation for multihistogram reweighting with AEs using the notation already introduced in Sec. II. Consider s different histograms $\mathcal{H}_1, \mathcal{H}_2, \ldots, \mathcal{H}_s$ collected from simulations performed at states defined by properties $\{D_j, \tilde{\mathbf{f}}_j\}$, $j = 1, \ldots, s$, respectively, and all for fixed $\bar{\mathbf{Y}}$. These histograms can be combined by using the Swedsen and Ferrenberg prescription [4]. One can then show that

$$\omega(U, \tilde{\mathbf{Y}} | \bar{\mathbf{Y}}) = \frac{\sum_{j=1}^{s} \mathcal{H}(U, \tilde{\mathbf{Y}} | D_j, \tilde{\mathbf{f}}_j | \bar{\mathbf{Y}})}{\sum_{j=1}^{s} \mathcal{K}_j W(U, \tilde{\mathbf{Y}} | D_j, \tilde{\mathbf{f}}_j) \exp(-\mathfrak{I}_j)} \tag{24}$$

where $\mathcal{K}_j$ is the number of entries in the jth histogram and the $\mathfrak{I}$ values are found self-consistently from

$$\mathfrak{I}_j = \ln\left(\int_{U,\tilde{\mathbf{Y}}} dU\, d\tilde{\mathbf{Y}}\ \omega(U,\tilde{\mathbf{Y}}|\bar{\mathbf{Y}}) W(U,\tilde{\mathbf{Y}}|D_j,\tilde{\mathbf{f}}_j) \right). \quad (25)$$

But since only $\mathfrak{I}$ differences are meaningful, one can set $\mathfrak{I}_1 = 0$. Equation (11) can be used to "extrapolate" the (unnormalized) probability of $\{U,\tilde{\mathbf{Y}}\}$ macrostates for arbitrary values of D and $\tilde{\mathbf{f}}$ (but the same $\bar{\mathbf{Y}}$). In Ref. [9] MHR was advantageously used to get ω even with ensemble-weight-independent approaches (i.e., when W does not individualize an IE or AE).

C. Estimating ω and $\mathfrak{I}$ with transition matrix methods

Transition matrix methods estimate ω and $\mathfrak{I}$ functions using simulation data on probabilities of attempted transitions (among microstates). Let macrostate I encompass a set of microstates or configurations ($i \in I$) that correspond to some prespecified value of the property ξ. This property can be any of those included in λ [Eq. (17)] but can also include U and other configuration-dependent order parameters; i.e., $\xi \subset \{D,\tilde{\mathbf{f}},\bar{\mathbf{Y}},U,\ldots\}$. If the probability density of a microstate is denoted by $p(i)$, then the probability of such a macrostate I is $\Pi(I) = \Sigma_{i\in I} p(i)$. Consider now two macrostates I and J each encompassing a number of configurations or microstates $\{i\}$ and $\{j\}$, respectively. The detailed balance condition for transitions between microstates i and j is

$$\alpha_{i,j} P_{acc}(i \to j) p(i) = \alpha_{j,i} P_{acc}(j \to i) p(j) \quad (26)$$

where $\alpha_{i,j} = \alpha(i \to j)$ and $P_{acc}(i \to j)$ are the probabilities of proposing and accepting the moves between microstates i and j, respectively. Starting from the equation above, it was shown in Ref. [54] that the "broad histogram" formula [55] and the generalized "Bennett's acceptance ratio" formula [56] are the same and take the form

$$\frac{\Pi(J)}{\Pi(I)} = \frac{C_{I,J}/n_I}{C_{J,I}/n_J} \quad (27)$$

where

$$n_K = \sum_{all\ L} \text{no. of attempts } K \to L, \quad (28)$$

$$C_{L,K} \equiv C_{L\to K} = \sum_{l\in L} (1 + \alpha_{l,k}/\alpha_{k,l}) P_{acc}(l \to k). \quad (29)$$

If $\xi \subset \{D,\tilde{\mathbf{f}},\bar{\mathbf{Y}}\}$ (i.e., $\xi = \lambda =$ the ME reaction coordinate), then a particular value of ξ (together with any other imposed constraints) determines a thermodynamic state and a partition function, so that $\ln \Pi(\xi_i) = \ln Q(\xi_i) = \mathfrak{I}_i$ [see Eq. (16)], and Eq. (27) is the (unoptimized) acceptance ratio method [57] to estimate free-energy differences. Of particular interest here, however, is the case when ξ is or includes U so that it does not determine a thermodynamic state. In such a case, if for all microstates $k \in K$ we assign the same average probability $\bar{p}(K)$, i.e.,

$$\bar{p}(K) = \langle p(k) \rangle \quad \forall\ k \in K, \quad (30)$$

then for any macrostate K there exists a density of states $\omega(K)$ associated with it:

$$\Pi(K) = \left(\sum_{k\in K} p(k) \right) = \bar{p}(K)\omega(K). \quad (31)$$

Consistent with Eqs. (11) and (12), in Eq. (31) and thereafter, ω may denote the excess (ω_{ex}) or the configutational function depending on whether or not ϖ_{ig} is included in $\bar{p}(K)$. Equation (31) can be seen as the definition of $\bar{p}(K)$. Substituting Eq. (31) into Eq. (27), we get

$$\frac{\omega(J)}{\omega(I)} = \frac{\bar{p}(J)^{-1} C_{I,J}/n_I}{\bar{p}(I)^{-1} C_{J,I}/n_J},$$

which can be conveniently rewritten as

$$\exp(S_J - S_I) = \frac{\omega(J)}{\omega(I)} = \frac{\hat{C}_{I,J}/n_I}{\hat{C}_{J,I}/n_J} \quad (32)$$

with

$$\hat{C}_{L,K} = \sum_{l\in L} (1 + \alpha_{l,k}/\alpha_{k,l}) \frac{P_{acc}(l \to k)}{P_{acc}(L \to K)}. \quad (32')$$

Here $P_{acc}(L \to K)$, which only depends on the macrostate values (not on the microstates), can take the Metropolis-rule form:

$$P_{acc}(L \to K) = P_K / \max[P_L, P_K], \quad (33)$$

or Baker's rule form [58]

$$P_{acc}(L \to K) = P_K / [P_L + P_K]. \quad (34)$$

If furthermore

$$p(k) = \bar{p}(K) \quad \forall\ k \in K, \quad (35)$$

and the α's are symmetrical ($\alpha_{i,j} = \alpha_{j,i}$), then $P_{acc}(l \to k) = P_{acc}(L \to K)$, and Eq. (32) simplifies to

$$\frac{\omega(J)}{\omega(I)} = \ln\left(\frac{n_{I,J}/n_I}{n_{J,I}/n_J} \right) \quad (36)$$

where $n_{I,J}(n_{J,I})$ is the number of times that a transition starting with a microstate belonging to $I(J)$ resulted in a microstate belonging to $J(I)$. Equation (36), a special case of Eq. (32), is a form of the broad-histogram formula [20]. The estimation of (relative values of) Π or ω from the use of Eq. (27), (32) or (36) is an overdetermined problem which has been described in detail and solved elsewhere [20,51,54] (it requires an optimization procedure where one minimizes the variance of the estimations of $\ln \Pi$).

The great appeal of Eq. (32) is that the sums $\hat{C}_{I,J}$ and n_I can be accumulated regardless of ensemble weight and could then be used to consolidate the contributions to ω from multiple simulation state points; e.g., from those performed in a ME wherein $\lambda \neq \xi$. To illustrate this idea, consider the case of an NVT simulation with $\xi = U$ (suitably discretized in bins) so that ω in Eq. (32) is $\omega(U|N,V)$. If we are interested in $\omega(U|N,V)$ over a broader range of U (for fixed N and V values), then one could run a ME$(T|NV)$ for multiple values of $\lambda = T$. From these simulations, one simply needs to accumulate the counters $\hat{C}_{I,J}$ and n_I (regardless of the value of T) and add them together to get ω via Eqs. (32) and (32′).

If ξ is a continuous variable and macrostates have been discretized into bins, then condition (35) does not strictly apply but if the bin width is not too wide one can use

$$\bar{p}(K) = \langle p(k) \rangle \approx p(\langle k \rangle), \tag{37}$$

i.e., each $\bar{p}(K)$ is evaluated at the average values of the k microstates belonging to bin K. Note that if one forces Eq. (35) to be obeyed, then Eq. (36) will give valid ω values but the simulated state points will no longer (exactly) correspond to the specified ensemble states (the calculation would then be analogous to a non-Boltzmann sampling scheme).

The most important application of Eq. (32) is when a macrostate is defined by combinations of values of all fluctuating properties in the ensemble; in that case ξ is a multidimensional vector

$$\xi = \{U, \tilde{\mathbf{Y}}\}, \quad \omega(\xi) = \omega_{ex}(U, \tilde{\mathbf{Y}} | \bar{\mathbf{Y}}), \tag{38}$$

so that $\Pi(K) = \Pi(U_K, \tilde{\mathbf{Y}}_K | D, \bar{\mathbf{Y}}, \tilde{\mathbf{f}})$ and $\bar{p}(K) \propto \varpi_{ig}(\tilde{\mathbf{Y}}_K | \mathbf{Y}) \times W(U_K, \tilde{\mathbf{Y}}_K | D, \tilde{\mathbf{f}})$, consistent with Eqs. (11) and (14). A key feature of Eq. (38) is that ω does not depend directly on any thermodynamic field used in the simulation.

IV. SIMULATION OF PHASE COEXISTENCE WITH MULTI-ENSEMBLES

In general, if we denote two phases as I and II, then at coexistence all thermodynamic fields must be the same:

$$\bar{f}_i^I = \bar{f}_i^I \equiv \bar{f}_i \quad \forall \bar{f}_i \subset \bar{\mathbf{f}}, \tag{39}$$

$$T^I = T^{II} \equiv T_{coex}. \tag{40}$$

And the equality of the fields in $\tilde{\mathbf{f}}$ can be established by direct specification. While there are several approaches to enact Eqs. (39) and (40) via simulation (e.g., via Gibbs ensembles [2,58,36]), we focus here on the use of MEs as a means to access the thermodynamic properties of a system, including phase equilibrium.

A. Isothermal ensembles

Several MEs have been used to map out phase coexistence with the IE (e.g., see [11–16]). The case when $\lambda = \beta$ [recall Eq. (17)] has been extensively used with an expanded ensemble and replica exchange (REX) algorithm (parallel tempering) [11–16] to improve conformational sampling and identify conformation transitions (e.g., in proteins). For completeness, we simply review another popular case of ME wherein one conducts a ME where T is fixed and only one extensive property $\lambda = Y_\lambda$ is varied: $Y_\lambda \cup \bar{\mathbf{Y}}' = \bar{\mathbf{Y}}$, so that each IE in the ME has partition function $Q(Y_\lambda) = Q(Y_\lambda, \bar{\mathbf{Y}}', \beta, \tilde{\mathbf{f}})$. Using methods such as those in Sec. III one can obtain the difference in the $\mathfrak{I}(Y_\lambda)$ values associated with these Q's. If f_λ is the field conjugate to Y_λ, one can then readily obtain the probability of Y_λ macrostates in the "expanded" ensemble $Q(f_\lambda) = Q(\bar{\mathbf{Y}}', \beta, \tilde{\mathbf{f}}, f_\lambda)$ from

$$\Pi(Y_\lambda | f_\lambda) = \exp[\mathfrak{I}(Y_\lambda) + \beta f_\lambda Y_\lambda] / Q(f_\lambda), \quad \text{fixed } \bar{\mathbf{Y}}', \beta, \tilde{\mathbf{f}}, \tag{41}$$

where

$$Q(f_\lambda) = \int dY_\lambda \Pi(Y_\lambda | f_\lambda). \tag{42}$$

Then if for a particular value of f_λ the $\Pi(Y_\lambda | f_\lambda)$ function exhibits a bimodal distribution with equal area under each hump, one has located a state where besides T, $\tilde{\mathbf{f}}$, and f_λ, also the free-energy function $\mathfrak{I}(f_\lambda) = \ln Q(f_\lambda) = -\beta \bar{\mathbf{f}}' \cdot \bar{\mathbf{Y}}'$ is the same in both phases. The latter implies phase coexistence if the vector $\bar{\mathbf{Y}}'$ (or $\bar{\mathbf{f}}'$) has only one component. This procedure has been employed for $Y_\lambda = N$, V, or $N_2 - N_1$ in several studies (e.g., in Refs. [21–25]).

B. Adiabatic ensembles

For concreteness, we only consider here a particular case of ME wherein just one extensive property is the reaction coordinate; namely, when $\lambda = D$ so that different states along the ME path correspond to different values of D (while $\tilde{\mathbf{f}}$ and $\bar{\mathbf{Y}}$ are fixed). Examples of this ME have been reported before [26] and extensions to multidimensional λ's can be pursued by following similar arguments. For the AEs, since $D = E - \tilde{\mathbf{f}} \cdot \tilde{\mathbf{Y}}$, using Eq. (2) we get

$$D = TS + \bar{\mathbf{f}} \cdot \bar{\mathbf{Y}}. \tag{43}$$

At phase coexistence where Eqs. (39) and (40) apply, Eq. (43) leads to

$$D^I - T_{coex} S^I = D^{II} - T_{coex} S^{II}. \tag{44}$$

And using Eq. (1) one finds [26]

$$T^{-1} = \left(\frac{\partial S}{\partial D} \right)_{\bar{\mathbf{Y}}, \tilde{\mathbf{f}}}, \tag{45}$$

$$\Delta S = \int T^{-1} dD, \quad \bar{\mathbf{Y}}, \tilde{\mathbf{f}} \text{ constant}, \tag{46}$$

which when integrated between D^I and D^{II} and combined with Eq. (44) leads to

$$\int_{D^I}^{D^{II}} \left(\frac{1}{T_{coex}} - \frac{1}{T} \right) dD = 0. \tag{47}$$

In a T^{-1} vs D plot, Eq. (47) can be seen as a generalized equal area Maxwell construction. Note that in AEs, the average T value for a given simulation point is obtained from [26]

$$kT = 2\langle K/(F-2) \rangle. \tag{48}$$

The ME$(D | \bar{\mathbf{Y}}, \tilde{\mathbf{f}})$ runs can generate relative values of $S/k = \ln \Omega(D | \bar{\mathbf{Y}}, \tilde{\mathbf{f}})$ by either the thermodynamic integration embodied by Eq. (46) or by using one of the methods in Sec. III.

The most complete and systematic AE$\leftrightarrow$IE connection is given by using as bridge the $\omega_{ex}(U,\tilde{\mathbf{Y}}|\bar{\mathbf{Y}})$ function as described in Sec. III. Another, albeit more limited, connection is to use Eq. (23) to go from AE runs with partition function $\Omega(\bar{\mathbf{Y}},\tilde{\mathbf{f}},D)$ and $\lambda=D=D_{AE}$ to simulation data for an IE with partition function $Q(\bar{\mathbf{Y}},\tilde{\mathbf{f}},\beta)$. Since differences in $S/k=\ln\Omega(D|\bar{\mathbf{Y}},\tilde{\mathbf{f}})$ are accessible from the ME$(D|\bar{\mathbf{Y}},\tilde{\mathbf{f}})$ runs, then Eq. (23) allows us to get the probability of D_{AB} macrostates $\Pi(D_{AE}|\bar{\mathbf{Y}},\tilde{\mathbf{f}},\beta)$ with which the average of a property X could be projected into the IE by using

$$\langle X\rangle_{\bar{\mathbf{Y}},\tilde{\mathbf{f}},\beta}\approx\int_{D_{AE}}dD_{AE}X(D_{AE},\bar{\mathbf{Y}},\tilde{\mathbf{f}})\Pi(D_{AE}|\bar{\mathbf{Y}},\tilde{\mathbf{f}},\beta). \quad (49)$$

Formulas (23) and (49), which are applicable within a limited range of temperatures (β) corresponding to the simulated D_{AE} domain, can be useful in pinpointing phase coexistence by allowing calculations for different T values (see Sec. VI).

V. SIMULATION DETAILS

All the simulation tests were performed for a single-component Lennard-Jones (LJ) system in a cubic box with periodic boundary conditions. All properties for this system will be reported dimensionless as they have been reduced by suitable combinations of the standard LJ energy ε and distance σ parameters and Boltzmann constant k [1,2]. The pairwise potential energy interactions were cut off at a distance of 2.5 and standard long-range tail correction added [2]. Configurational sampling (at constant volume) consisted of translation moves where randomly chosen particles attempt to move in a random direction by a maximum distance d_{max}. The value of d_{max} was chosen to maintain an acceptance rate in the 30–40% range. Volume moves, when needed, entailed incremental expansions or contractions of the simulation box dimensions while the positions of the particles were rescaled by maintaining their reduced coordinates (with respect to the box length) unchanged [2]. The maximum volume change $|\Delta V_{max}|$ was tuned to give a 30% acceptance rate. Both translation and volume moves (going from microstate o to n) were accepted using the Metropolis criterion

$$P_{acc}=\min\left(1,\frac{\varpi_{ig,n}W_n}{\varpi_{ig,o}W_o}\right). \quad (50)$$

Because Eq. (32) overspecifies ω ratios for any given pair of macrostates, optimal values were obtained via an explicit order-N formula described in Ref. [54].

Most ME simulations were performed using a replica exchange algorithm. For REX, the $\bar{\mathbf{Y}}$ properties in λ [Eq. (17)] are fixed so that each individual replica corresponds to an ensemble with a distinct $\lambda\in\{D,\tilde{\mathbf{f}}\}$. The overall partition function for N_s replicas with such a REX scheme is $Q^*(\lambda)=\prod_{i=1}^{N_s}Q(\lambda_i)$ and the probability density of a λ state is

$$\Pi(\lambda_i)=Q(\lambda_i)/Q^*(\lambda). \quad (51)$$

To sample states according to Eq. (51), we performed configurational moves as described above and "swap" moves between neighboring replicas. If a swap is attempted between replicas i and j having identical $\bar{\mathbf{Y}}$ parameters but with $\lambda_i=\{D_i,\tilde{\mathbf{f}}_i\}$ and $\lambda_j=\{D_j,\tilde{\mathbf{f}}_j\}$, and having microstates $\gamma_i=\{\tilde{\mathbf{Y}}_i,\mathbf{r}_i\}$ and $\gamma_j=\{\tilde{\mathbf{Y}}_j,\mathbf{r}_j\}$, respectively, then the Metropolis rule is

$$P_{acc}=\min\left[1,\frac{W(\lambda_j,\gamma_i)W(\lambda_i,\gamma_j)}{W(\lambda_i,\gamma_i)W(\lambda_j,\gamma_j)}\right], \quad (52)$$

Successive λ values were manually chosen so that P_{acc} ranged between 0.1 and 0.3. Note that our ME runs did not need to be performed in parallel with REX; however, this improves ergodic sampling and gives as a by-product the values of $\Delta\mathfrak{I}$. In fact, the change in property $\mathfrak{I}$ [see Eq. (16)] between any pair of neighboring states i and j can be readily obtained with Bennett's method, at no extra cost, from the replica swap attempts by simply using Eq. (27) and realizing that $\mathfrak{I}(\lambda_i)=\ln\Pi(\lambda_i)$ with $\lambda_i=\xi_i$. In our applications, the $\mathfrak{I}$'s thus obtained were almost indistinguishable from those obtained from the self-consistent MHR relation [Eq. (25)].

VI. RESULTS

Because N will always be constant in the ensuing applications, we will omit it in the notation of ω, S, and ME so that, e.g., $\omega(U|N,V)$ will just appear as $\omega(U|V)$.

A. Targeting the ω density of states

First we demonstrate the AI-AE connection of Eq. (21) by using as AI the *NVT* ensemble and as AE the *NVE* ensemble (see Table I). Note that for either ensemble, ω_{ex} and ω agree within a constant factor. In both cases, $F=3N$ and $\bar{\mathbf{Y}}=\{N,V\}$ with $N=110$ LJ particles and $V=125$ (liquid-like density); the ME runs involved 10 state points and 3×10^5 cycles per replica where each cycle consisted of 250 translation moves and 1 swap move. Also in both cases, we targeted the $\omega(U|V)$ function in the range of U from -700 to -500 using a discretized scale with $\Delta U=1$ (i.e., 200 macrostates). For the *NVT* runs, the temperatures were 0.73, 0.84, 0.97, 1.11, 1.28, 1.47, 1.69, 1.94, 2.23, and 2.57 (approx. $T_{i+1}=1.15T_i$) which gave REX swap acceptance rates between 20% and 30%. For the *NVE* runs, the energies were -600, -572, -540, -505, -465, -418, -360, -290, -210, and -110; the REX swap acceptance rates ranged between 12% and 15%. For these two MEs, the $P_{acc}(L\to K)$ (for translation moves) were discretized (with $\Delta U=1$) to allow the collection of $\hat{C}_{I,J}$ data for direct use with Eq. (32) to get $\omega(U|V)$. For comparison, additional conventional MEs were conducted where $\omega(U|V)$ was obtained via the MHR Eqs. (24) and (25) [instead of Eq. (32)].

Figure 1 shows the results for the incremental values of $\ln\omega$ obtained for the ME$(T|V)$ runs. Clearly ω obtained via Eq. (32) ME agrees quantitatively with that obtained with the conventional ME [obtained via the MHR Eq. (24)], although the latter exhibits noticeable larger noise than the former. The improved statistical accuracy in ω estimates from TM methods [like Eq. (32)] relative to those from visited-states

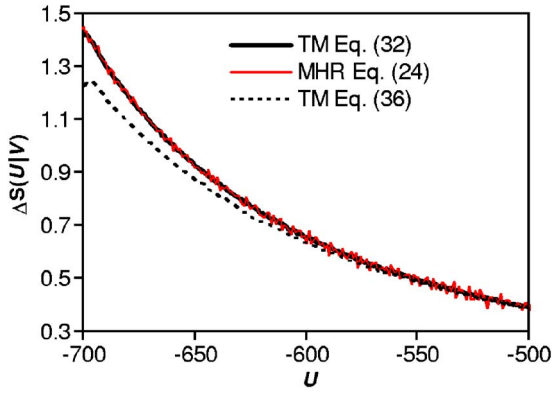

FIG. 1. (Color online) Density of states function $\ln \omega(U|V)$ for the LJ fluid obtained from ten *NVT* ensemble runs (for $T=0.73$, 0.84, 0.97, 1.11, 1.28, 1.47, 1.69, 1.94, 2.23, and 2.57) and fixed $N=110$, $V=125$. Results are shown for the MHR technique [gray (red) lines], for the correct TM method [Eq. (32), full lines], and for the "incorrect" TM method [Eq. (36), dashed lines].

methods (like MHR) has been thoroughly quantified before [20,51,54]. The importance of using the appropriate $\hat{C}_{I,J}$ definition is illustrated by obtaining ω via Eq. (36) instead of the "correct" Eq. (32); clearly, Eq. (36) leads to results exhibiting systematic errors. Similar outcomes were obtained when we performed the corresponding comparison with data from adiabatic ME runs (not shown). Further, the ω values obtained from isothermal MEs agree completely with those from adiabatic MEs, whether one uses Eq. (32) or Eq. (24) (with the latter always exhibiting larger noise). This agreement is illustrated in Fig. 2 where we show that the energy histograms for several temperatures collected with the standard isothermal MEs, match well those reweighted [e.g., with Eq. (11)] from the ω obtained via Eq. (32) with the adiabatic ME.

The simulations described above were also used to test the validity of Eq. (19). Because the results for $\omega \propto \omega_{ex}(U|V)$ found before (from either ME series) targeted the U range $[-700,-500]$, the two integration limits in Eq. (19) pose some limitations: (1) the resulting $\Omega(E|V)$ will be approximate because ω_{ex} is not known down to $U \to \infty$ (lower limit), and (2) we can only get results for Ω up to $E=-500$ (upper limit). In Fig. 3 we plot the results obtained from this integration and for $\mathfrak{I}=S/k=\ln \Omega(E|V)$ as obtained from the use of Eq. (27) for the ME$(E|V)$ REX swaps. It can be seen that both sets of data agree well in the overlapping range of E.

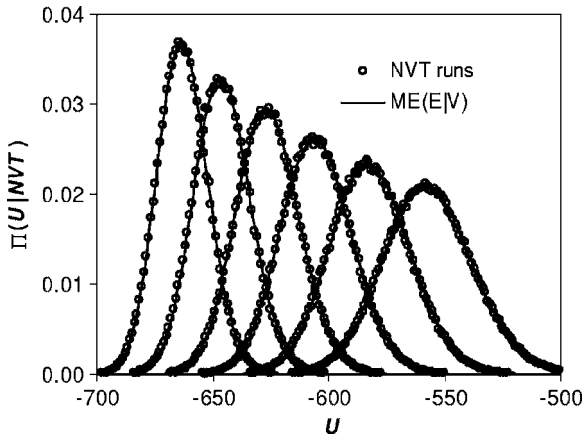

FIG. 2. Comparison of energy histograms for the LJ fluid obtained from standard canonical simulations for temperatures 0.97, 1.11, 1.28, 1.47, 1.69, and 1.94 (circles) and by reweighting of the $\omega(U|V)$ function obtained from ME$(E|N,V)$ (lines). The latter comprised ten runs with $E=-600$, -572, -540, -505, -465, -418, -360, -290, -210, and -110. In all cases $N=110$, $V=125$.

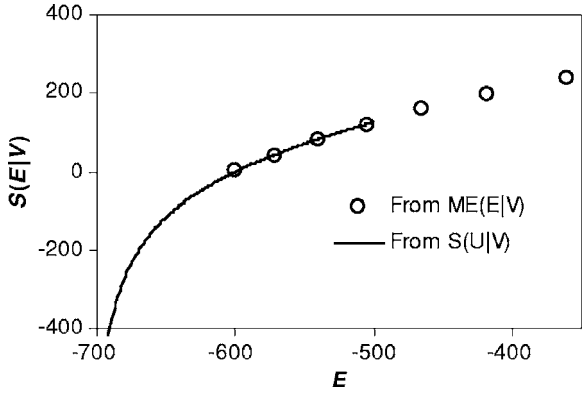

FIG. 3. Comparison of the simulated entropy $[\ln \Omega(E|V)]$ for the LJ fluid as obtained from multiple *NVE* runs (circles) and from the integration [via Eq. (19)] of the $\omega(U|V)$ data shown in Fig. 1 (lines).

If we are interested in obtaining a "two-dimensional" (2D) $\omega(U,V)$ over a broad $\{U,V\}$ domain, an economic way to do so is by assembling several $\omega(U|V)$ isochores, generated for different volumes, via multiple *NVE* or *NVT* runs. Such a "multiple 1D paths" approach to ω has been illustrated before [54] wherein the $\omega(U|V)$ isochores were first found using an (ensemble-weight-independent) multicanonical-type TM method, and then "stitched" together via a ME$(V|T)$ run. Of course, one can use instead multiple *NVE* or *NVT* ensemble runs to get the $\omega(U|V)$ curves (instead of an ensemble-weight-independent approach). We tested two such schemes for the $N=128$ LJ system, one relying exclusively on IEs and the other on AEs. Since the results from both are comparable, we will only describe the adiabatic scheme wherein we used ME$(E|V)$ runs to get the isochoric ω's and stitched them with a ME$(V|E)$ run. For each volume, we performed the ME$(E|V)$ using REX with 28 E values ranging from -600 to $+1400$ (with intervals gradually increasing), monitored the U range between -806ε and 64ε discretized in 435 bins ($\Delta U=\Delta\xi=2$), and used Eq. (32) to get $\omega(U|V)$; each ensemble state was run for 15 000 cycles, where each cycle consisted of attempting 700 translations and four REX swaps. We simulated 40 such isochores for volumes ranging from 129.43 to 9878.4 with a nearly logarithmic spacing. For the (stitching) volume-varying ME run, we let V adopt 195 discrete values in the same range as before with $V_i=127.996 \exp[0.022\,345(i-0.5)]$ for $i=1,2,\ldots,195$. In this case we used a serial ME wherein volume transitions involved only two neighbor ensembles at a time (similar to

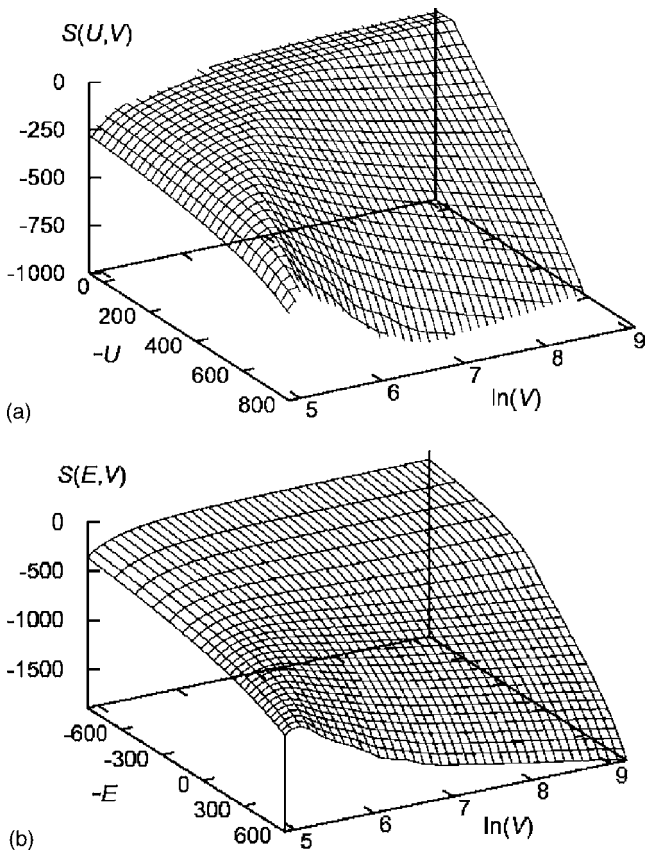

FIG. 4. (a) Excess $S(U,V)$ surface and (b) excess $S(E,V)$ surface for the LJ fluid ($N=128$). Both surfaces were extracted from a series of ME($E|V$) runs, each for a different volume and spanning 28 different values of E (from −600 to 1400). The stitching ME($V|E$) run was with $E=150$ and spanned 195 different values of V (from 129.4 to 9878.4). The surfaces can be shifted vertically by an arbitrary amount.

"successive umbrella sampling" [59]) so that in average, every ensemble point was run for 15 000 cycles, each consisting of attempting 200 single-particle translations and eight volume changes. For this stitching ME, we set $E=E_s=150$ and used Eq. (27) to obtain the ratios of successive $\Pi(V)$ values.

The scheme described above also allows us to get $\Omega(E,V)$ if we collect the $\Delta\mathfrak{I}=\Delta S(E|V)$ values from the REX swaps (isochoric runs). The stitching can be done by using

$$S(E,V) = S(E|V) + [S(V|E_s) - S(V_0|E_s)] - [S(E_s|V) - S(E_s|V_0)] \quad (53)$$

where V_0 is an arbitrary volume used as reference, and the terms in the first square brackets are from the ME($V|E_s$) run while all the others in the right hand side of Eq. (53) are from the ME($E|V$) runs. To get $S(U,V)=k\ln\omega(U,V)$, it can be shown that the stitching can be done with

$$S(U,V) = S(U|V) + [S(V|E_s) - S(V_0|E_s)] - [\underline{S}(E_s|V) - \underline{S}(E_s|V_0)] \quad (54)$$

where the $\underline{S}$ terms are found by integration of the simulated

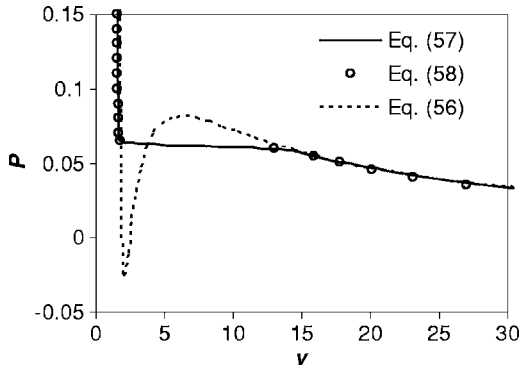

FIG. 5. $T=1.15$ isotherm for the $N=128$ LJ system obtained by finding the average specific volume (v) for preset T and P via Eq. (57) (full lines) and Eq. (58) (circles). Also shown is the isotherm found via Eq. (56) applied to the surface of Fig. 4(b) (dotted lines) which, unlike the previous two, does show a van der Waals loop (consistent with a saturation pressure of ~0.062).

$\omega(U|V)=\exp[S(U|V)]$ data [from the ME($E|V$) run] via Eq. (19); i.e.,

$$\underline{S}(E_s|V) = \ln\Omega(E_s|V) = \ln\left(\int_{-\infty}^{E_s} dU'\,\omega(U'|V)(E_s-U')^{F/2-1}\right). \quad (55)$$

Figure 4(a) shows the excess part of the $S(U,V)$ function [i.e., it does not include the ideal ($N\ln V$) contribution] which agrees quantitatively with that reported before (e.g., in [50,54]). Figure 4(b) shows our results for the corresponding excess $S(E,V)$ surface which, compared to $S(U,V)$, exhibits similar rough trends (e.g., larger S for larger energies) but has a very different local topography. In the $S(U,V)$ surface, the "difficult" region is that of larger volumes and more negative energies because it corresponds to inhomogeneous states where molecules form cluster and interfaces; our simulation scheme is able to sample that region more comprehensively than other approaches [e.g., the one based on ME($T|V$) runs, or the one used in [50]]. Because the E increments are much larger than the U increments, the $S(E,V)$ surface is defined over a coarser grid than the $S(U,V)$ surface; however, one could use interpolation methods to get S at any point inside the domains. Also, the stitching procedure of the multiple 1D paths (which circumvents a full 2D sampling scheme) is more straightforward for $S(E,V)$.

Despite the difference between $S(U,V)$ and $S(E,V)$, both can be used (once ideal gas contributions are added) to generate all key thermodynamic properties; e.g., from

$$T^{-1} = (\partial S/\partial E)_V, \quad P = T(\partial S/\partial V)_E, \quad (56)$$

and $G=E+PV-TS$. Also, they can be used to estimate the macrostate probability density for given P and T; i.e., from Eq. (11) applied to the NPT ensemble,

$$\Pi(U,V|P,T) \propto \exp[S(U,V)/k - U/kT - PV/kT] \quad (57)$$

and from Eq. (22)

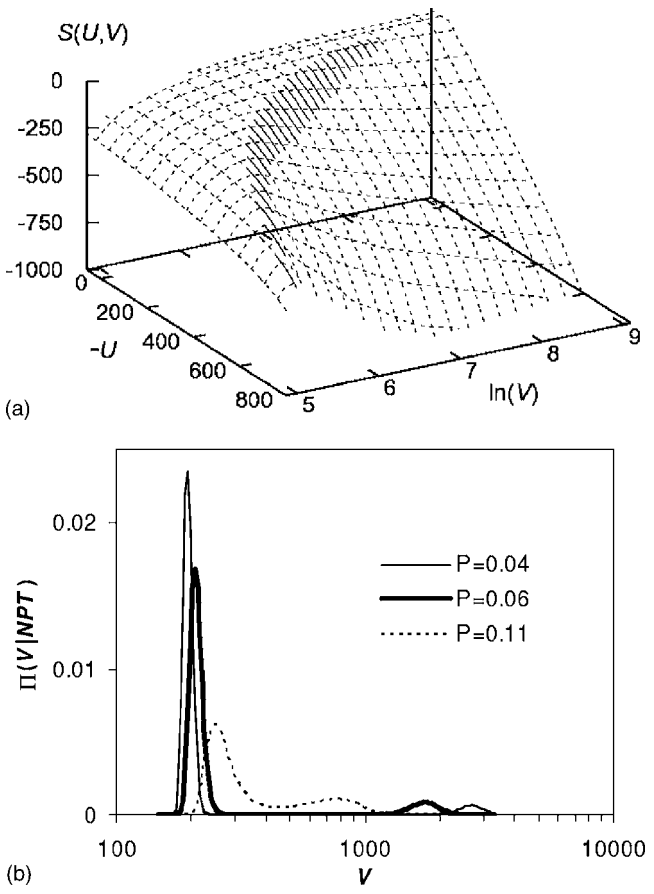

FIG. 6. Results from a ME($H|P$) run with $P=0.06$ and 25 H values (from −560 to +400) for the $N=128$ LJ fluid. (a) Excess $S(U,V)$ surface from this ME is shown by full lines; for reference, the surface from Fig. 4(a) is also shown by dotted lines. (b) Volume probability density at coexistence for three pressures obtained from the S of Fig. 6(a); the equal-area criterion is satisfied by each bimodal curve although this is distorted by the logarithmic scale of V.

$$\Pi(E,V|P,T) \propto \exp[S(E,V)/k - E/kT - PV/kT] \qquad (58)$$

with which average properties $\langle X\rangle = \int X\Pi(U,V)dU\,dV$ and $\langle X\rangle = \int X\Pi(E,V)dE\,dV$ can be found. Figure 5 shows PV data for a subcritical isotherm found using Eqs. (56)–(58). Although phase coexistence could be estimated from such isotherms, Eqs. (57) and (58) allow a more direct route via the "equal-probability-volume" criterion wherein one finds P-T pairs of values that give a bimodal probability density having equal "volume" (total probability) under each peak. Unreported sample coexistence results using Eqs. (57) and (58) [see, however, Fig. 6(b)] agree with each other and with those given in Ref. [50]. Note that $\Pi(U+K,V|P,T)$ from Eq. (57) with $K=3NkT/2$ (a maximum term approximation) is not the same as $\Pi(E,V|P,T)$ from Eq. (58) since the former does not capture the variability of K.

We can also sample a portion of $\omega(U,V)$ via simulations in an ensemble where both U and V are allowed to fluctuate like the NPT and NPH ensembles. We illustrate this calculation using a ME with NPH ensembles and $\lambda=H$, i.e., a ME($H|P$) (see Table I). We use the same $N=128$ LJ system as before and use a subcritical pressure $P=0.06$ and H values ranging from −560 to +400 with 25 points (step size of 40); in this way, the simulated points go from liquid states to vapor states. The ME was run for 5×10^4 cycles/replica, where each cycle consisted of 800 translation moves, five volume moves, and four REX swaps. In this case each macrostate is defined by the values of U and V, a case consistent with Eq. (38). In implementing Eq. (32), U was collected in bins with a width of $\Delta U=2$ and the volume was discretized so that allowable values lie on a logarithmic scale: $\ln V_i = 0.022\,345i + \text{const}$. Such a discretization of V is done for convenience and is not essential; one could use instead a continuous V and classify their values into discrete bins (as is done with U). To obtain $S(U,V)$ from Eq. (32) we used the method described in the Appendix (with V=property 1 and U=property 2).

A plot of the excess S surface thus obtained is shown in Fig. 6(a) which is overlaid on that of Fig. 4(a). Clearly the ME($H|P$) run used here is able to sample only a small portion of S that lies just below the flat upper terrace toward the drop region. However, this small region is an interesting one because, by virtue of our selection of P and H values, we have targeted the liquid and vapor states in and around the binodal curve. We show this by using Eq. (57) to pinpoint coexistence data via the equal-probability-volume criterion. Figure 6(b) shows the marginal $\Pi(V|P,T)$ histograms at coexistence (i.e., for equal-area peaks) found from the ME($H|P$)-derived $S(U,V)$ function for three pressures: 0.06 (the one used in the ME run), 0.04, and 0.11 (as close to the critical point as is sensible). The estimated coexistence temperatures for these pressures are very close though, as expected from our small system size, consistently lower (by 0.6%) than those obtained from the Lotfi *et al.* correlation [60]. If it is desired to estimate coexistence conditions for even lower pressures, one simply needs to add more points at the ends of the H spectrum in our ME($H|P$) to collect $S(U,V)$ data relevant to denser liquids and lighter vapors. While $\omega(U,V)$ can come from NPH runs or NPT runs [61], the key advantage of using the former is that they readily sample macrostates inside the bimodal curve (two-phase region) and therefore allow connecting vapor and liquid states and pinpoint phase coexistence without having to do a bridge around or near the critical point (a similar advantage exists in using a $VL\mu$ ME over a $VT\mu$ ME).

The same calculations associated with Fig. 6 can be carried out if one collects macrostate histograms and uses the MHR Eq. (24) rather than the TM Eq. (32), though the former always gives noisier results. We illustrate such a MHR implementation using the same ME($H|P$) approach used before but for a larger LJ system with $N=250$ to facilitate comparison with previously reported data [26,62]. We thus set $P=0.06$ with states that ranged from $H=-1000$ to +700 with 35 equally spaced points. The ME was run for 5×10^4 cycles/replica, where each cycle consisted of 800 translation moves, six volume moves, and two REX swaps. We collected histograms (of U and V) for each of the 35 states and used Eq. (24) to obtain $\omega(U,V)$:

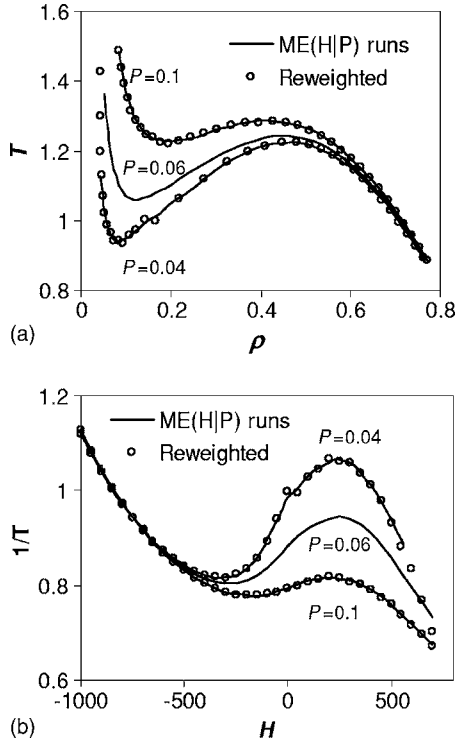

FIG. 7. Two representation of three isobars for the LJ fluid ($N=250$) obtained from ME($H|P$) runs (lines) wherein for each pressure the simulations spanned 35 values of H (from −1000 to 700). MHR extrapolations from the $P=0.06$ ME are shown by circles.

$$\omega(U,V) = \frac{\sum_{j=1}^{s} \mathcal{H}(U,V|H_j,P_j)}{\sum_{j=1}^{s} \mathcal{K}_j W(U,V|H_j,P_j)\exp(-S_j/k)}, \quad (24')$$

where W is given in Table I, and S_j is the (relative) entropy of the jth state [found from either Eq. (25) or from Bennett's Eq. (27) applied to the REX swaps]. We then obtained the probability density of macrostates at other conditions of H and P, from

$$\Pi(U,V|H,P) \propto \omega(U,V)W(U,V|H,P), \quad (11')$$

and from these we got $\langle T\rangle_{NPH}$ and $\langle\rho\rangle_{NPH}$. The T vs ρ results thus reweighted for $P=0.04$ and 0.1 are shown in Fig. 7 and compared against the data obtained from direct simulation at those pressures. Clearly, the extrapolations agree well with the direct simulation data. Just as was done in Fig. 6(b), we could also get accurate coexistence results for $0.035<P<0.11$.

B. Pinpointing phase coexistence with adiabatic Ω's (without ω)

If $\omega(U,V)$ is known over a sufficiently large domain as in Figs. 4(a) and 6(a), then most of the vapor-liquid coexistence curve can be readily mapped out via the equal-probability-volume criterion as was done in Ref. [50] and illustrated in Fig. 6(b). Here, however, we consider an alternative scenario where the ω is unknown but Ω (or S) is accessible in some domain. This may correspond to cases where ω depends on numerous variables and we are only interested in a limited region of a phase diagram. To illustrate this "targeted" approach, we use as a basis the ME($H|P$) simulation results obtained before for the LJ system at $P=0.06$ and $N=250$, and H values ranging from −1000 to +700. For convenience, we list several methods that can be used.

(1) Maxwell construction—thermodynamic integration. This involves the use of Eq. (47) which in this case is $\int_{H_L}^{H_V}(1/T_{coex}-1/T)dH=0$. This construction, illustrated in Fig. 8(a), only requires knowledge of $T(H)$ simulation data [which embody S data as per Eq. (46)].

(2) Double-tangent construction. This is based on Eqs. (44) and (45) so that the points H_V and H_L (at phase coexistence) must satisfy $(\partial S/\partial H_L)_{N,P}=(\partial S/\partial H_V)_{N,P}=1/T_{coex}$ and $-G_{coex}/T_{coex}=S_V-H_V/T_{coex}=S_L-H_L/T_{coex}$. This implies that if one draws the $S(H)$ curve, straight lines tangent at the vapor and liquid equilibrium points must have the same slope and intercept; i.e., they fuse into a line that is simultaneously tangent at both points. This construction, illustrated in Fig. 8(b), only requires the knowledge of $S(H)$ simulation data.

(3) The "intersection" or chemical potential method. This is based on Eq. (44) that can be used to get the chemical potential from

$$\mu(H) = [H - T(H)S(H)]/N.$$

A plot of $\mu(H)$ vs T (or T^{-1}) should show phase coexistence as an intersection point between two branches: at that point one has equality of both the temperature (x axis) and the chemical potential (y axis) for the phases representing these two branches. This construction is illustrated in Fig. 8(c) and requires knowledge of both $T(H)$ and $S(H)$ data from simulation.

(4) The ensemble projection method. This is based on the AE-to-IE transformation described by Eqs. (23) and (49). Phase coexistence is estimated by detecting the signs of a first-order transition in an IE. In our case, the relevant transformation is to go from NPH data to NPT data. The first variant (method 4a) is based on Eq. (23) which in this case reads

$$\Pi(H|P,T) \propto \exp[S(H)/k - H/kT] \quad (59)$$

where constancy of N and P is implicit in $S(H)$. To find the coexistence point for the given P, one reweights $\Pi(H|P,T)$ using Eq. (59) until finding a T for which an equal-area bimodal histogram is obtained. This construction, illustrated in Fig. 8(d), only requires the knowledge of $S(H)$ data from simulation. In a second variant of this method (4b), we look for a discontinuity in the free-energy derivative; e.g., on the average density vs T (along an isobar). Using Eqs. (49) and (59), we can get $\langle\rho\rangle_{NPT}$ at fixed N, P, and T from $\langle\rho\rangle_{NPT}=\int_H \rho(H)\Pi(H|P,T)dH$. A plot of $\langle\rho\rangle_{NPT}$ vs T is illustrated in Fig. 8(e). It requires data of $S(H)$ and $\rho(H)$ from simulation. Note that no actual discontinuity in $\langle\rho\rangle_{NPT}$ is seen at a particular T (T_{sat}), but rather a sharp drop. A third variant of this method (4c) involves monitoring the divergence of a second-order derivative of G; e.g., in the heat capacity found from

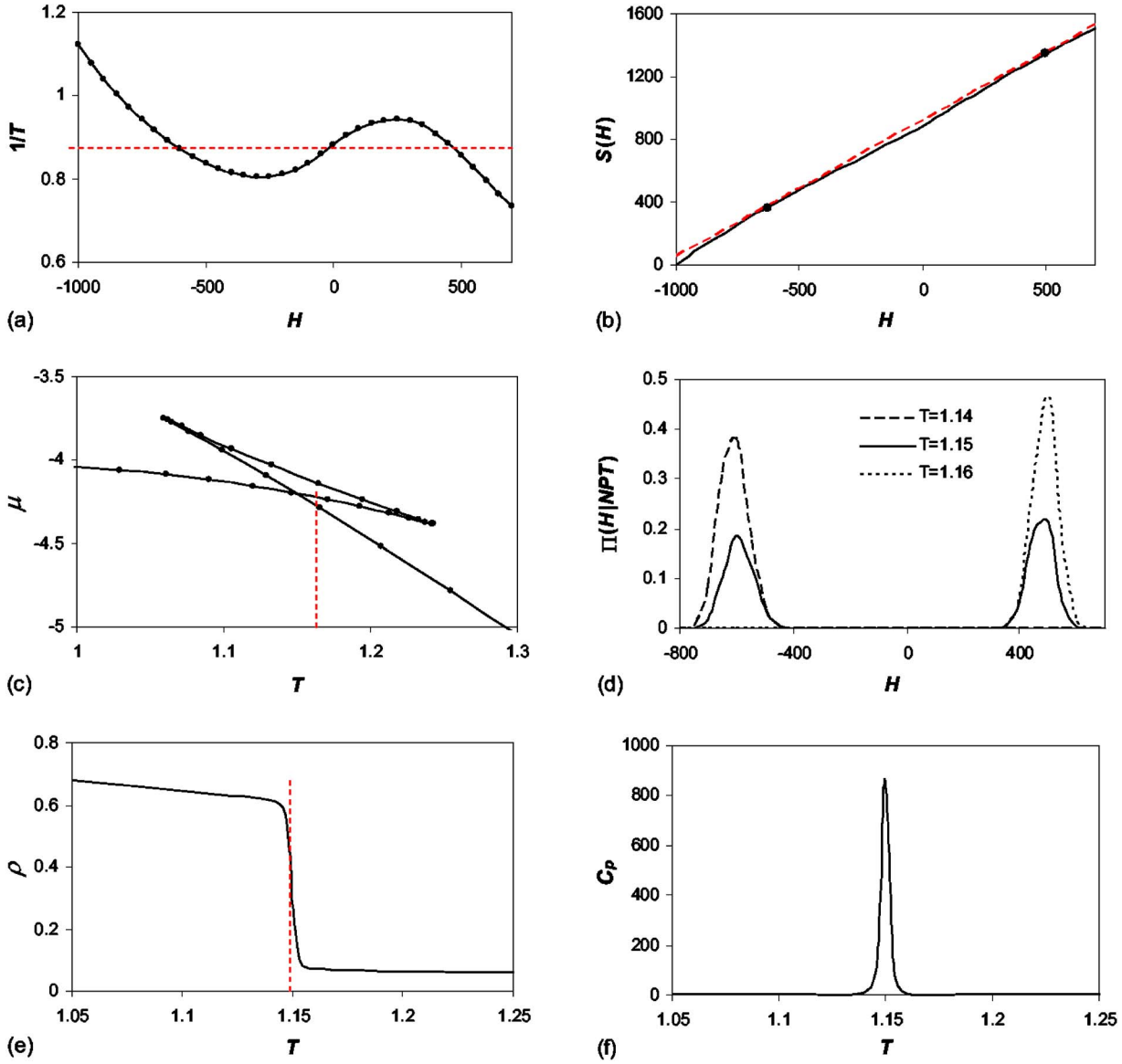

FIG. 8. (Color online) Illustration of different approaches to estimate coexistence conditions from ME($H|P$) runs. Data are for the LJ fluid with $N=250$ and $P=0.06$. In (a), (b), and (c) T refers to the temperature in the NPH ensemble runs; i.e., $T=\langle T\rangle_{NPH}$, while in (d), (e), and (f) T refers to an input temperature used to evaluate the system properties [like $p(H)$, ρ, and C_p] at NPT conditions.

$$C_p = \frac{1}{kT^2}(\langle H^2\rangle_{NPT} - \langle H\rangle_{NPT}^2), \tag{60}$$

where each expectation value in Eq. (60) is found from Eq. (49). T_{coex} is at the point where $\langle C_p\rangle_{NPT}$ vs T exhibits a sharp peak. This construction, illustrated in Fig. 8(f), only requires knowledge of $S(H)$ simulation data.

All the methods above agree (within error bars) on giving $T_{coex}\sim 1.15\pm 0.002$ which in turn agrees with accepted results [60]. Note that in terms of raw simulation data needed for the determination, methods 2, 4a, and 4c are equivalent [need $S(H)$ data only], method 1 uses the most readily accessible data [$T(H)$ only], and methods 3 and 4b require more data [$S(H)$ and either $T(H)$ or $\rho(H)$, respectively]. Unlike methods that obtain $\omega(U,V)$, none of the methods listed here allows estimation of coexistence data at pressures other than the one used in the ME($H|P$) runs; for example, one could apply Maxwell's construction (method 1) to the isobars of Fig. 7(b) to obtain T_{coex} for $P=0.04$ and $P=0.1$. It is noted that methods 1 and 3 were used in Ref. [26] to estimate vapor-liquid and solid-liquid coexistence in pure and binary systems.

VII. CONCLUSIONS

We have presented the common statistical mechanical basis for the simulation of the density of states in an arbitrary ensemble. Building on a robust notation system previously used to describe AEs, we have given a unified formulation of the partition function of both AEs and IEs and presented general formulas that encapsulate different methods involved in obtaining the density of states ω_{ex} from simulations of

AEs and IEs. Once ω_{ex} is obtained, whether it was from IE or AE runs, we showed that one can reweight ω_{ex} via Eq. (11) to obtain probability densities and other properties for the suitable ensemble. For example one could go from *NVT* (multi)ensemble data $\rightarrow \omega_{ex}(U|N,V) \rightarrow$ *NVE* ensemble data, or vice versa; i.e., from *NVE* (multi)ensemble data $\rightarrow \omega_{ex}(U|N,V) \rightarrow$ *NVT* ensemble data.

Using the Lennard-Jones system as a testbed, we have applied and compared the calculation of ω based on MHR (a visited-states method) and a TM scheme (a transition probability method). We found that the latter generates results with less statistical noise than the former, an advantage that has been associated with TM methods before and is expected to hold for more complex systems. We have also shown that by a suitable generalization of the acceptance-ratio method one arrives at a simple formula [Eq. (32)] that allows the information on microstate transitions from different simulation points to be simply added to global counters. In this way, the TM route to ω is not only more accurate than the MHR route but it provides a convenient bookkeeping scheme to consolidate all the statistical data needed to get ω.

Unlike multiple *NPT* runs (for varying T), the use of multiple *NPH* runs (for varying H) allows one to bridge two coexistence phases for any P. This leads to the collection of a more complete ω function for the reweighting of data over a broad range of T and P; in particular, to obtain vapor-liquid coexistence data over a wide pressure range. Finally, we illustrated the use of different approaches to pinpoint vapor-liquid coexistence in the LJ fluid from the information of multiple *NPH* runs at constant pressure. Such methods are not confined to the *NPH* ensemble nor to pure components and could be especially valuable in cases where insertion or deletion of particles is troublesome (e.g., for large or cyclic molecules).

It is expected that the IE $\leftrightarrow \omega_{ex} \leftrightarrow$ AE connection will help identify instances where one can harness the strengths of AIs and AEs. Generating $S(E,V)$ rather than $S(U,V)$, for example, may be advantageous in some cases. While we focused on mapping $S(U,V)$ and $S(E,V)$, similar approaches can be used to map $S(U,N)$ and $S(E,N)$. For convenience, we have employed the simplest possible systems to validate the advocated methods. Some algorithmic refinements may be needed to simulate systems with more components or with macrostates defined by structure-dependent order parameters. For example, within the framework of REX and Bennett's acceptance-ratio methods, data from virtual swap moves could be used to optimize the estimation of the $\mathfrak{J}$ or ω function as was done in Ref. [63].

ACKNOWLEDGMENTS

Support is acknowledged from the Sloan Foundation and from the National Science Foundation, Grant No. BES-0093769.

APPENDIX: IMPLEMENTATION OF EQ. (32) FOR A 2D DOMAIN

The determination of S differences from Eq. (32) is an overdetermined problem because for any macrostates I and J, $S_J - S_I$ can be found not only from the direct transitions between I and J but also from the results of other jumps; i.e., via any path that starts at I and ends at J in more than 1 step. The solution to the problem of finding "optimal" S differences has been described before for cases when a "macrostate" is defined by the values of a single macrovariable [20,51,54]. It involves the minimization of the total variance of the estimation of S differences via a least-squares analysis. In principle, the same procedure can be used when each macrostate is defined by two or more macrovariables but the size of the arrays can become very large and cumbersome to handle. We describe here an alternative procedure for a case with two macrovariables that takes advantage of the fact that for one of the macrovariables, denoted here "property 1," transitions can at most take the system between macrostates having neighboring values of such a property. Property 1 could be for instance V or any other property (like N) whose values (and transition between them) can be directly specified. On the other hand, "property 2" is a macrovariable like U for which transition end points cannot be directly specified (due to its coupling with the system configuration).

Every macrostate can then be specified by two indexes so that the terms $\hat{C}$ and n in Eq. (32) are denoted $\hat{C}(i,\Delta i,j,k)$ and $n(i,\Delta i,j)$ where the index i gives the current state of property 1, and Δi gives its change as a result of by the proposed transition; $\Delta i = \pm 1$ if a change in property 1 is proposed and $\Delta i = 0$ otherwise. The indices j and k denote the current and new values of property 2, respectively. The entropy change associated with any transition $\{i,j\} \rightarrow \{i+\Delta i,k\}$ is therefore denoted as $S(i+\Delta i,k) - S(i,j)$. Instead of solving for all the optimal S values at once, we adopted the following two-step process.

(1) Find first the optimal $S(i,k) - S(i,j)$ values, i.e., for every "slice" of macrophase space with fixed value of property 1. For each value of i (and with $\Delta i = 0$), this involves the solution of a 1D problem for the $\{i,j\} \rightarrow \{i,k\}$ transitions which is identical to previous applications of the optimization method and to the one we used to get S in Fig. 1 (where V was fixed and only transitions between U macrostates were considered). In the present case Eq. (32) takes the form

$$S(i,k) - S(i,j) = \ln\left(\frac{\hat{C}(i,0,j,k)/n(i,0,j)}{\hat{C}(i,0,k,j)/n(i,0,k)} \right). \qquad \text{(A1)}$$

The redundancy in the information on $\{i,j\} \rightarrow \{i,k\}$ transitions was used to estimate optimal $S^*(i,k) - S^*(i,j)$ values as reported in Ref. [54] (the asterisks are used to denote optimal S values found in this step).

(2) Find the relative shifts δS between successive S slices found in step 1; i.e.,

$$\delta S_{i+1} = S^{opt}(i+1,k) - S^{opt}(i,k) - [S^*(i+1,k) - S^*(i,k)] \quad \forall \; k. \qquad \text{(A2)}$$

In other words, δS_{i+1} is the quantity that we need to add to $S^{opt}(i,k)$ to get the best value for the next slice $S^{opt}(i+1,k)$. Note that the differences $[S^*(i+1,k) - S^*(i,k)]$ obtained from step 1 are arbitrary. Meaningful estimates for $[S(i+1,k) - S(i,k)]$ can be obtained from transitions that involved

changes of property 1 (only) between values i and $i+1$; these can be estimated using Eq. (32):

$$\Delta S_{j,k} = S(i+1,k) - S(i,j) = \ln\left(\frac{\hat{C}(i,+1,j,k)/n(i,+1,j)}{\hat{C}(i+1,-1,k,j)/n(i+1,-1,k)} \right). \quad \text{(A3)}$$

Thus estimates for the δS shift can be found from

$$\delta S_{i+1} = \Delta S_{j,k} - \Delta S^*_{j,k}$$

where $\Delta S_{j,k}$ is from Eq. (A3) and $\Delta S^*_{j,k} = S^*(i+1,k) - S^*(i,j)$. Since δS must be the same regardless of the values of property 2 (i.e., for any j and k values), we can find the optimal shift δS^{opt}_{i+1} by minimizing the total variance given by

$$\sigma^2_{i,tot} = \sum_{j,k} \frac{[\delta S^{opt}_{i+1} - (\Delta S_{j,k} - \Delta S^*_{j,k})]^2}{\sigma^2_{j,k}} \quad \text{(A4)}$$

where

$$\sigma^2_{j,k} = 1/\hat{C}(i,+1,j,k) + 1/\hat{C}(i+1,-1,k,j) + 1/n(i,+1,j) + 1/n(i+1,-1,k). \quad \text{(A5)}$$

Setting $d\sigma^2_{i,tot}/d(\delta S^{opt}_{i+1}) = 0$ we find the sought-after solution:

$$\delta S^{opt}_{i+1} = \sum_{j,k} \frac{(\Delta S_{j,k} - \Delta S^*_{j,k})}{\sigma^2_{j,k}} \Bigg/ \sum_{j,k} \frac{1}{\sigma^2_{j,k}}. \quad \text{(A6)}$$

Once δS^{opt}_{i+1} is found, one then uses Eq. (A2) to find the optimal values for $S^{opt}(i+1,k)$ for all k values, and going sequentially from $i=2,3,\ldots$, having set $S^{opt}(1,k) = S^*(1,k)$. Note that in some respects, this two-step procedure is reminiscent of the multiple 1D paths+stitching approach described in Sec. VI (regarding Fig. 4), except that here the ME run involved 2D transitions so that the information for the stitching (step 2 here) does not require a separate run. This two-step process is not restricted to ME runs but can also be applied to ensemble-weight-independent multicanonical-type simulations and generalized for more than two macro variables.

[1] M. P. Allen and D. J. Tildesley, *Computer Simulation of Liquids* (Clarendon Press, Oxford, 1987).
[2] D. Frenkel and B. Smit, *Understanding Molecular Simulation: From Algorithms to Applications* (Academic, San Diego, 2000).
[3] A. M. Ferrenberg and R. H. Swendsen, Phys. Rev. Lett. **61**, 2635 (1988).
[4] A. M. Ferrenberg and R. H. Swendsen, Phys. Rev. Lett. **63**, 1195 (1989); P. Labastie and R. L. Whetten, *ibid.* **65**, 1567 (1990).
[5] N. B. Wilding, Phys. Rev. E **52**, 602 (1995).
[6] A. Z. Panagiotopoulos, J. Phys.: Condens. Matter **12**, R25 (2000).
[7] J. J. de Pablo, Q. Yan, and F. A. Escobedo, Annu. Rev. Phys. Chem. **50**, 377 (1999).
[8] A. D. Bruce and N. B. Wilding, Adv. Chem. Phys. **127**, 1 (2003).
[9] C. H. Abreu and F. A. Escobedo, J. Chem. Phys. **124**, 054116 (2006).
[10] C. Bartels, M. Schaefer, and M. Karplus, J. Chem. Phys. **111**, 8048 (1999).
[11] P. Lyubartsev, A. A. Martinovski, S. V. Shevkunov, and P. N. Vorontsov Velyaminov, J. Chem. Phys. **96**, 1776 (1992).
[12] N. B. Wilding and M. Muller, J. Chem. Phys. **101**, 4324 (1994).
[13] F. A. Escobedo and J. J. de Pablo, J. Chem. Phys. **103**, 2703 (1995).
[14] M. C. Tesi, E. J. J. van Rensburg, E. Orlandini, and S. G. Whittington, J. Stat. Phys. **82**, 155 (1996).
[15] U. H. E. Hansmann, Chem. Phys. Lett. **281**, 140 (1997).
[16] Q. Yan and J. J. de Pablo, J. Chem. Phys. **111**, 9509 (1999); **113**, 1276 (2000).
[17] M. Fitzgerald, R. R. Picard, and R. N. Silver, Europhys. Lett. **46**, 282 (1999).
[18] M. Fitzgerald, R. R. Picard, and R. N. Silver, J. Stat. Phys. **98**, 321 (2000).
[19] G. R. Smith and A. D. Bruce, J. Phys. A **28**, 6623 (1995).
[20] J.-S. Wang and R. H. Swendsen, J. Stat. Phys. **106**, 245 (2002).
[21] J. R. Errington, Phys. Rev. E **67**, 012102 (2003).
[22] J. R. Errington, J. Chem. Phys. **118**, 9915 (2003).
[23] M. K. Fenwick and F. A. Escobedo, J. Chem. Phys. **119**, 11998 (2003).
[24] M. K. Fenwick and F. A. Escobedo, J. Chem. Phys. **120**, 3066 (2004).
[25] I. D. Gospodinov and F. A. Escobedo, J. Chem. Phys. **122**, 164103 (2005).
[26] F. Escobedo, J. Chem. Phys. **123**, 044110 (2005).
[27] H. W. Graben and J. R. Ray, Phys. Rev. A **43**, 4100 (1991).
[28] H. W. Graben and J. R. Ray, Mol. Phys. **80**, 1183 (1993).
[29] M. Parrinello and A. Rahman, Phys. Rev. Lett. **45**, 1196 (1980).
[30] J. R. Ray and H. W. Graben, J. Chem. Phys. **75**, 4077 (1981).
[31] J. R. Ray, Phys. Rev. A **44**, 4061 (1991).
[32] J. R. Ray and H. W. Graben, J. Chem. Phys. **93**, 4296 (1990).
[33] R. Lustig, J. Chem. Phys. **109**, 8816 (1998).
[34] Z. Zhou, J. Chem. Phys. **114**, 8769 (2001).
[35] T. Kristof and J. Liszi, Chem. Phys. Lett. **261**, 620 (1996).
[36] T. Kristof and J. Liszi, Mol. Phys. **94**, 519 (1998).
[37] L. Merenyi and T. Kristof, Mol. Phys. **30**, 549 (2004).
[38] F. Calvo and P. Labastie, Chem. Phys. Lett. **247**, 395 (1995).
[39] F. Calvo and P. Labastie, Eur. Phys. J. D **3**, 229 (1998).
[40] F. Calvo, J. P. Neirotti, D. L. Freeman, and J. D. Doll, J. Chem. Phys. **112**, 10350 (2000).
[41] F. Calvo, Mol. Phys. **100**, 3421 (2002).
[42] L. I. Kioupis, G. Arya, and E. J. Maginn, Fluid Phase Equilib. **200**, 93 (2002).
[43] B. A. Berg and T. Neuhaus, Phys. Rev. Lett. **68**, 9 (1992).
[44] B. A. Berg and T. Celik, Phys. Rev. Lett. **69**, 2292 (1992).
[45] J. Lee, Phys. Rev. Lett. **71**, 211 (1993); **71**, 2353 (1993).

[46] F. Wang and D. P. Landau, Phys. Rev. Lett. **86**, 2050 (2001).
[47] F. Wang and D. P. Landau, Phys. Rev. E **64**, 056101 (2001).
[48] Q. Yan, R. Faller, and J. J. de Pablo, J. Chem. Phys. **116**, 8745 (2002).
[49] Q. Yan and J. J. de Pablo, Phys. Rev. Lett. **90**, 035701 (2003).
[50] M. S. Shell, P. G. Debenedetti, and A. Z. Panagiotopoulos, Phys. Rev. E **66**, 056703 (2002).
[51] M. S. Shell, P. G. Debenedetti, and A. Z. Panagiotopoulos, J. Chem. Phys. **119**, 9406 (2003).
[52] F. A. Escobedo, J. Chem. Phys. **15**, 5642 (2001).
[53] W. H. Press, W. T. Vetterling, S. A. Teukolsky, and B. P. Flannery, *Numerical Recipes in Fortran 77: The Art of Scientific Computing*, 2nd ed. (Cambridge University Press, New York, 2001), p. 786.
[54] F. A. Escobedo and C. H. Abreu, J. Chem. Phys. **124**, 104110 (2006).
[55] P. M. C. de Oliveira, T. J. P. Penna, and H. J. Herrmann, Braz. J. Phys. **26**, 677 (1996).
[56] C. H. Bennett, J. Comput. Phys. **22**, 245 (1976).
[57] A. A. Barker, Aust. J. Phys. **18**, 119 (1965).
[58] A. Z. Panagiotopoulos, Mol. Phys. **61**, 813 (1987).
[59] P. Virnau and M. Muller, J. Chem. Phys. **120**, 10925 (2004).
[60] A. Lofti, J. Vrabec, and J. Fischer, Mol. Phys. **76**, 1319 (1992).
[61] P. B. Conrad and J. J. de Pablo, Fluid Phase Equilib. **150**, 51 (1998).
[62] In Ref. [26], the data for $P=0.02$ in Figs. 4 and 5 are for a system with 200 (not 250) particles.
[63] I. Coluzza and D. Frenkel, ChemPhysChem **6**, 1779 (2005).